Comparison of Two Airfoil Sections for Application in Straight-Bladed Darrieus VAWT

Marco Raciti Castelli and Ernesto Benini

Abstract—This paper presents a model for the evaluation of energy performance and aerodynamic forces acting on a small straight-bladed Darrieus-type vertical axis wind turbine depending on blade geometrical section. It consists of an analytical code coupled to a solid modeling software, capable of generating the desired blade geometry based on the desired blade design geometric parameters. Such module is then linked to a finite volume commercial CFD code for the calculation of rotor performance by integration of the aerodynamic forces along the perimeter of each blade for a full period of revolution. After describing and validating the computational model with experimental data, the results of numerical simulations are proposed on the bases of two candidate airfoil sections, that is a classical symmetrical NACA 0021 blade profile and the recently developed DU 06-W-200 non-symmetric and laminar blade profile. Through a full CFD campaign of analysis, the effects of blade geometrical section on angle of attack are first investigated and then the overall rotor torque and power are analyzed as a function of blade azimuthal position, achieving a numerical quantification of the influence of airfoil geometry on overall rotor performance.

Keywords—Wind turbine, NACA 0021, DU 06-W-200.

I. INTRODUCTION AND BACKGROUND

THE vertical axis wind turbine has an inherently non-stationary aerodynamic behavior, mainly due to the continuous variation in the blade angle of attack during its rotation: this peculiarity involves the continuous variation both of the relative velocity (and related angle of attack) with respect to the blade profile and - although to a lesser extent - of the corresponding Reynolds number. This phenomenon, typical of slow rotating machines, has a significant effect both on the dynamic loads acting on the rotor and on the generated power.

Classical aerodynamic tools such as the actuator disc concept and the directly derived theory of blade elements (BE-M) [1] [2] [3], while presenting the advantage of a low computation effort, are nevertheless limited by the availability of extended airfoil databases (up to 180°) which should also refer to rather low local Reynolds numbers (close to Re = 10^5), which are typical of a vertical axis wind turbine operation.

Since most airfoil databases available in literature are derived from aeronautical applications, hardly extending far beyond stall and also referring to relatively high Reynolds numbers (above Re = 10^6), it has been recognized that there is a paucity of accurate airfoil data needed to describe the aerodynamics of wind turbine blades. The airfoil section data

Marco Raciti Castelli is Research Associate at the Department of Mechanical Engineering of the University of Padua, Via Venezia 1, 35131 Padova, Italy (e-mail: marco.raciticastelli@unipd.it).

Ernesto Benini is Associate Professor at the Department of Mechanical Engineering of the University of Padua, Via Venezia 1, 35131 Padova, Italy (e-mail: ernesto.benini@unipd.it).

requirements for application in vertical axis wind turbines are in fact broader in scope than those the aircraft industry usually concerns itself with. This limits the analysis on vertical axis wind turbines to a narrow number of blade profiles, substantially some NACA series of symmetrical airfoils, for which extended databases at low Reynolds numbers are available in literature [4]. Moreover, as pointed out by Burton et al. [5], dwelling upon considerations on the energy extraction process rather than on the specific turbine design, all classical aerodynamic tools are unable to visualize the basic structure of the flow field inside the rotor volume.

So far, high quality wind tunnel data is required to verify the aerodynamic design of a rotor, in order to obtain the operating torque curves for the implementation of the control system. Advanced computational methods could nevertheless provide a highly efficient means of maturing initial concept studies into effective aerodynamic designs that meet target operational objectives. In CFD simulations, a computer essentially replaces the physical simulation in the wind tunnel: CFD methods involve very large amounts of computation even for relatively simple problems and their accuracy is often difficult to assess when applied to a new problem where previous experimental validation has not been done [6]. Anyway, performing CFD calculations provide knowledge about the flow in all its details, such as velocities, pressure, temperature, etc. Furthermore, all types of useful graphical presentations, such as flow lines, contour lines and iso-lines are readily available. This stage can be compared to having completed a wind-tunnel study or an elaborate full-scale measurement campaign [7].

As suggested by Raciti Castelli [8], the limitations in low Reynolds number accurate aerodynamic databases can be overcame by the use of CFD codes which can outflank the lack of airfoil data thanks to their inherent ability to determine the aerodynamic components of actions through the integration of the Navier-Stokes equations in the neighborhood of the wind turbine blade profile.

Till now Ferreira [9] [10] presented a systematic CFD analysis of a two-dimensional blade configuration. The effect of dynamic stall in a 2D single-bladed VAWT was investigated, reporting the influence of the turbulence model in the simulation of the vortical structures spread from the blade.

Raciti Castelli and Benini [11] presented a model for the evaluation of energy performance and aerodynamic forces acting on a helical single-bladed VAWT depending on blade inclination angle and based on five machine architectures, which were characterized by an inclination of the blades with respect to the horizontal plane in order to generate a phase shift angle between lower and upper blade sections of 0°, 30°, 60°, 90° and 120° for a rotor with aspect ratio of 1.5.

World Academy of Science, Engineering and Technology
International Journal of Aerospace and Mechanical Engineering
Vol:5, No:12, 2011

Anyway a single bladed VAWT, although very suitable for the visualization of flow field close to the rotor and for the performance comparison between several candidate rotor blade architectures, has no practical engineering applications: in order to numerically simulate the operation of a three-bladed VAWT, also analyzing blade mutual effects on relative angles of attack, Raciti Castelli et al. [12] transferred to a CFD code the basic principles which are currently applied to BE-M theory for rotor performance prediction, allowing the correlation between flow geometric characteristics, such as blade angles of attack, and dynamic quantities, such as rotor torque and blade tangential and normal forces. Through the coupling of the Ffowcs-Williams and Hawkings acoustic model to the described VAWT performance prediction model, Raciti Castelli et al. [13] performed also numerical simulations in order to evaluate the effect of the central shaft on overall rotor noise emission, showing marked oscillations in the measured acoustic values due to the passage of the downwind blade into the wake generated from the rotor shaft itself, thus causing a low frequency pulsation whose period is connected to rotor angular velocity.

In the present paper, an application of the performance prediction model described in [12] is presented, in order to demonstrate the capability of the proposed procedure, based on the analysis of kinematic and dynamic quantities at discrete and fixed rotor azimuthal positions along blades trajectory: a full comparative two-dimensional CFD campaign of analysis is completed for two candidate rotor blade architectures:

- a straight-bladed Darrieus rotor made of three classical symmetric NACA 0021 airfoils, named *Model 1*;
- a straight-bladed Darrieus rotor made of three recently-developed DU 06-W-200 non-symmetric and laminar airfoil, designed in 2006 at Delft University of Technology [14], named *Model 2*;

The effects of blade geometrical section on angle of attack and blade tangential forces are first numerically investigated; next, the basic structure of the flow field, the overall rotor torque and power are analyzed as functions of the blade azimuthal position, achieving a numerical quantification of the influence of airfoil geometry on overall rotor performance.

II. MODEL GEOMETRY

Fig. 1 shows a scheme of the survey methodology utilized, consisting in the coupling of an analytical code to a solid modeling software, capable of generating the desired rotor geometry depending on the desired design geometric parameters, which is linked to a finite volume CFD code for the calculation of rotor performance. CFD results are postprocessed using a second analytical code for calculation of rotor main kinematic and dynamic characteristics.
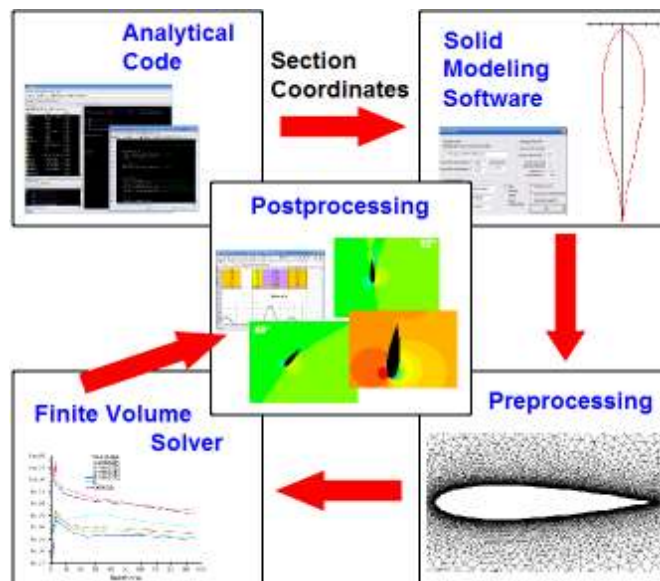

Fig. 1 Schema of the survey methodology (from: [12]).

The aim of this work was to numerically analyze the aerodynamic behavior of a 2D vertical-axis three-bladed Darrieus wind turbine operating inside a wind tunnel of 4000 mm width. The main geometric characteristics of the two analyzed blade profile sections are summarized in Table 1.

TABLE I
AIRFOIL SECTION MAIN FEATURES OF THE TWO TESTED MODELS

Model Name	Blade Section	c [mm]
Model 1	NACA 0021	85.8
Model 2	DU 06-W-200	85.8

The common features of the tested rotors are summarized in Table II. The solidity parameter σ is defined as Nc/R_{rotor}, as suggested by Strickland [3].

TABLE II
COMMON FEATURES OF THE TWO TESTED MODELS

Denomination	Value
R_{rotor} [mm]	515
H_{rotor} [mm]	1 (2D simulation)
N [-]	3
c [mm]	85.8
Spoke-blade connection	0.25 c
σ [-]	0.5

Fig. 2 compares the geometries of the classical NACA 0021 airfoil [15] with the non-symmetric and laminar DU 06-W-200 one [14].
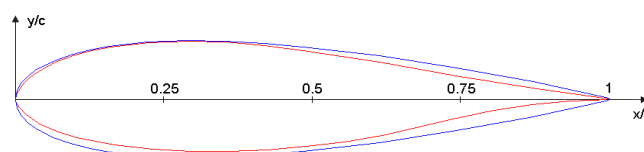

Fig. 2 Comparison between classical NACA 0021 (blue) and DU 06-W-200 (red) normalized airfoils

World Academy of Science, Engineering and Technology
International Journal of Aerospace and Mechanical Engineering
Vol:5, No:12, 2011

The DU 06-W-200 airfoil main features are the following [14]:

- added thickness of 2% with respect to NACA 0018, from which it is derived;
- added camber of 0.8% with respect to a symmetrical airfoil;
- performance similar to NACA 0018 for negative angles of attack and much higher maximum lift coefficient for positive angles of attack;
- higher deep stall angles of attack with respect to NACA 0018.

Rotor azimuthal position was identified by the angular coordinate of the pressure centre of blade No. 1 midsection (set at 0.25•c), starting between the 2nd and 3rd Cartesian plane octants, as can be seen in Fig. 3.

Fig. 4 Low turbulence wind tunnel at the "Politecnico di Milano" (source: [16]); the proposed simulations reproduce the operation of the rotor inside the test section (evidenced by the red circle).
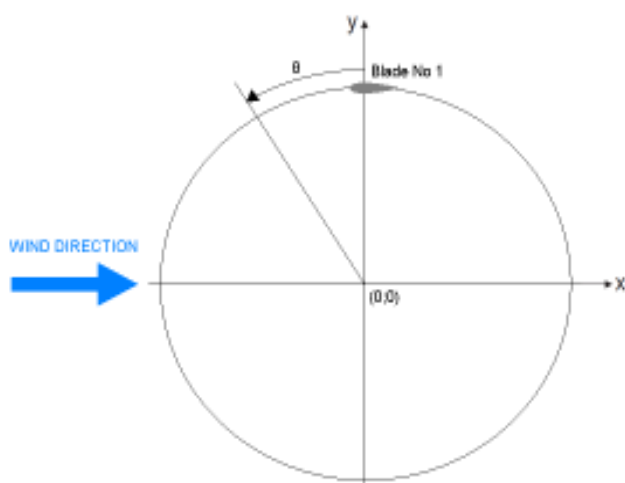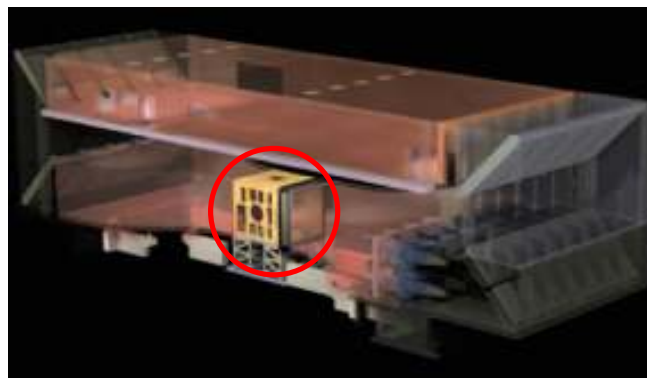

Fig. 3 Azimuthal coordinate of blade No. 1 midsection's centre of pressure (from: [12]).

III. Spatial Domain Discretization

The proposed simulations are based on wind tunnel measurements made in Milano-Bovisa's low turbulence facility [16] (Figure 4) on a straight-bladed Darrieus rotor, made of three NACA 0021 airfoils having a chord length of 85.8 mm, constructed of aluminum and carbon fibers.

Before analyzing the models described in the current section, a complete validation work based on wind tunnel measurements has been conducted [17]. Comparison of the computed results with experimental data showed that prediction obtained using *Enhanced Wall Treatment k-ε Realizable* turbulence model successfully reproduced most of the flow features associated with the revolution of the tested rotor. In particular, the numerical code proved able to replicate the shape of the experimental curve and was able to accurately capture the maximum power coefficient tip speed ratio, thus offering a reliable alternative to the development of experimental tests, at least at a first attempt.

The two analyzed models have kept the same main features of the validation model: a computational domain of rectangular shape was chosen, having the same wind tunnel external sizes. The wall boundary conditions of the model consisted in two lateral walls spaced 2000 mm apart from the wind tunnel centerline (the wind tunnel measured 4000 mm in width and 3880 mm in height). The rotor axis was placed on the symmetry position of the wind tunnel section. All the meshes analyzed in the present work had common geometric features, except for the areas close to the blade profiles.

As the aim of the present work was to reproduce the operation of a rotating machine, the use of moving sub-grids was necessary. In particular, the discretization of the computational domain into macro-areas has led to two distinct sub-grids:

- a rectangular outer zone, determining the overall calculation domain, with a circular opening centered on the turbine rotational axis, which was identified as Wind Tunnel sub-grid, fixed;
- a circular inner zone, which was identified as Rotor sub-grid, rotating with rotor angular velocity ω.

A. Wind Tunnel sub-grid

Fig. 5 shows the main dimensions and the boundary conditions of the Wind Tunnel sub-grid area.

Inlet and outlet boundary conditions were placed respectively 10 rotor diameters upwind and 14 rotor diameters downwind with respect to the rotor, allowing a full development of the wake, in accordance to what suggested by the work of Ferreira et al [9].

Two wall boundary conditions were used for the two side walls. The circumference around the circular opening, centered on the turbine rotational axis, was set as an interface, thus ensuring the continuity of the flow field.

An unstructured mesh was chosen for the Wind Tunnel sub-grid, in order to reduce engineering time to prepare the CFD simulations.

World Academy of Science, Engineering and Technology
International Journal of Aerospace and Mechanical Engineering
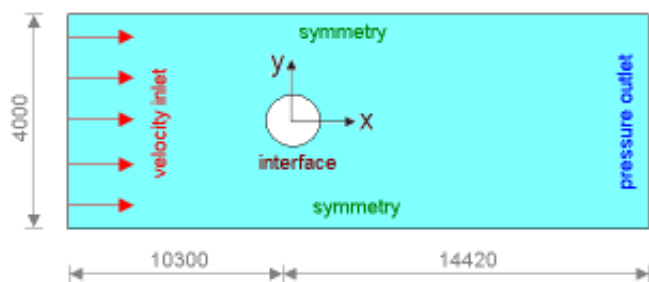Vol:5, No:12, 2011

Fig. 5 Main dimensions [mm] of the Wind Tunnel sub-grid area

B. Rotor sub-grid

The Rotor sub-grid is the fluid area simulating the revolution of the wind turbine and is therefore characterized by a moving mesh, rotating at the same angular velocity of the turbine. Its location coincides exactly with the circular opening inside the Wind Tunnel sub-grid area and centered on the turbine rotational axis.

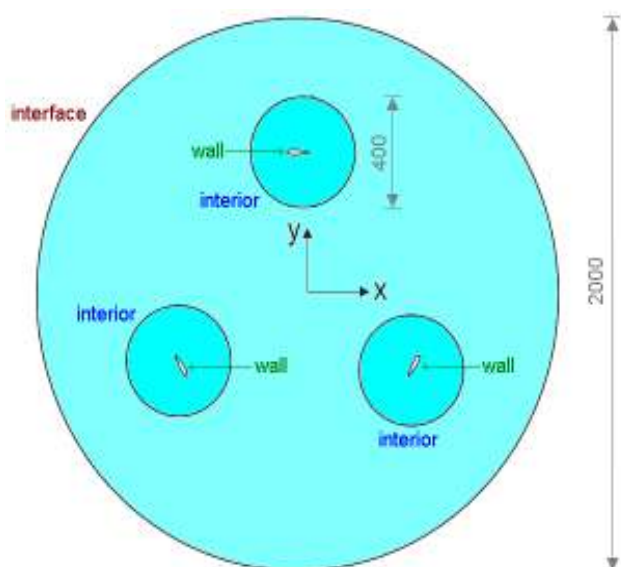Fig. 6 shows the main dimensions and the boundary conditions of the Wind Tunnel sub-grid area.

Fig. 6 Scheme [mm] of Rotor sub-grid area (from: [12])

It is good engineering practice to provide that the mesh on both sides of the interface (Rotor sub-grid and Wind Tunnel sub-grid areas) has approximately the same characteristic cell size in order to obtain faster convergence [18].

An isotropic unstructured mesh was chosen for the Rotor sub-grid, in order to guarantee the same accuracy in the prediction of rotor's performance during the revolution – according to the studies of Cummings et al. [19] – and also in order to test the prediction capability of a very simple grid. Considering their features of flexibility and adaption capability, unstructured meshes are in fact very easy to obtain, for complex geometries, too, and often represent the "first attempt" in order to get a quick response from the CFD in engineering work.

All blade profiles inside the Rotor sub-grid area were enclosed in a control circle of 400 mm diameter. Unlike the interface, it has no physical significance: its aim is to allow a precise dimensional control of the grid elements in the area close to rotor blades by adopting a first size function operating from the blade profile to the control circle itself and a second size function operating from the control circle to the whole Rotor sub-grid area, ending with grid elements of the same size of the corresponding Wind tunnel sub-grid elements. An interior boundary condition was used for control circle borders, thus ensuring the continuity of the cells on both sides of the mesh.

A growth factor of 1.26 was set from the surface of the control circle to Rotor sub-grid, thus expanding grid size from 4 mm to 10 mm, as shown in Fig. 7.
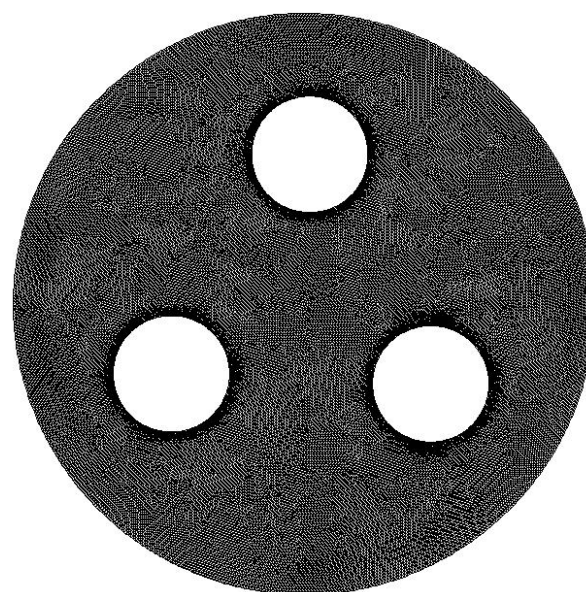

Fig. 7 Rotor sub-grid mesh (from: [12])

IV. THE CONTROL CIRCLE

Being the area close to the blade profiles, most attention was placed to the control circle. All the differences between the various meshes adopted in the present work were concentrated in this area. Figs. 8 and 9 compare the grids in correspondence of the control circle for both *Model 1* and *Model 2* rotor blades.

Table III summarizes the main features of the mesh close to rotor blade.

The computational grids were constructed from lower topologies to higher ones, adopting appropriate size functions, in order to cluster grid points near the leading edge and the trailing edge of the blade profile, so as to improve the CFD code capability of determining lift, drag and the separation of the flow from the blades itself.
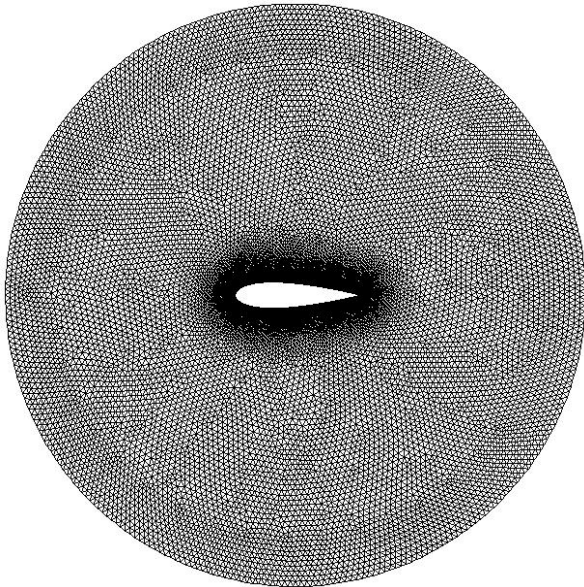
World Academy of Science, Engineering and Technology
International Journal of Aerospace and Mechanical Engineering
Vol:5, No:12, 2011

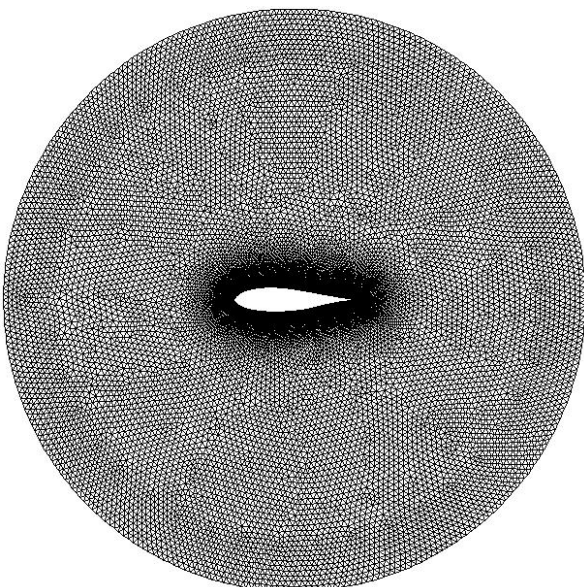Fig. 8 Control circle grid for *Model 1* rotor blade section (from: [12])

Fig. 9 Control circle grid for *Model 2* rotor blade section

TABLE III
MAIN FEATURES OF THE MESH CLOSE TO ROTOR BLADE (FROM: [12])

Denomination	Value
Number of grid points on airfoil upper/lower surface [-]	3600
Minimum grid points spacing (on airfoil leading edge) [mm]	0.015
Maximum grid points spacing (on airfoil trailing edge) [mm]	0.025
Growth factor from airfoil leading edge to airfoil trailing edge [-]	1.005
Growth factor from airfoil surface to Rotor sub-grid area [-]	1.1

Two size functions were set inside the control circle, as shown in Fig. 10:

- size function No. 1 starts from the leading edge and influences inner and outer blade profile;
- size function No. 2 starts from the blade profile and influences the whole control cylinder area, as described in the previous section.

The trailing edge thickness was set to about 0.38 mm. 10 grid points were placed in the trailing edge, as shown in Figure 11.
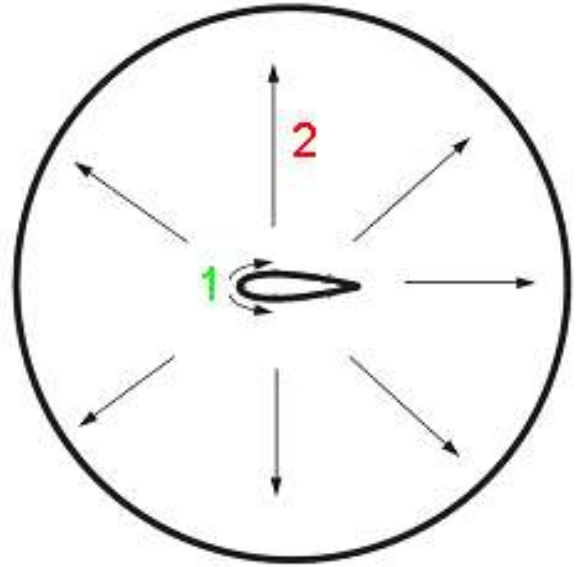

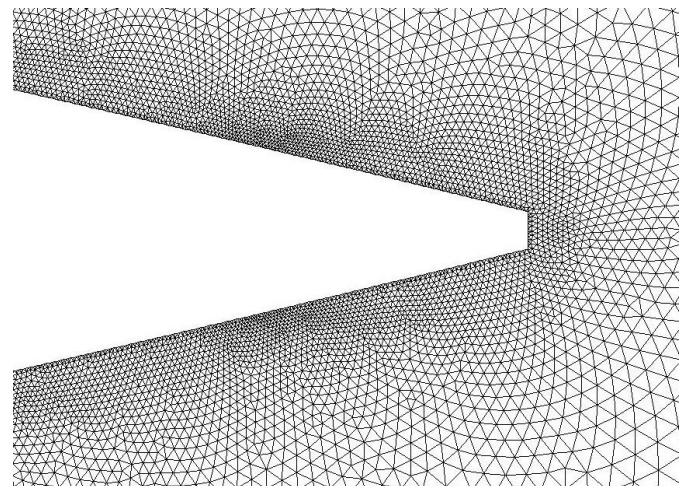Fig. 10 Size functions applied to control circle elements (from: [12]).

Fig. 11 Grid points clustering close to trailing edge for rotor Model 1 blade section.

V. TEMPORAL DISCRETIZATION AND CONVERGENCE CRITERIA

As a global convergence criterion, each simulation has been run until instantaneous torque coefficient values showed a deviation of less than 1% compared with the relative values of the previous period, corresponding to a rotation of 120° due to rotor three-bladed geometry. Residuals convergence criterion for each physical time step has been set to 10^{-5}.

The adopted commercial CFD package was Fluent 6.3.26, that implements 2-D Reynolds-averaged Navier-Stokes equations using a finite volume-finite element based solver. The fluid was assumed to be incompressible, being the maximum fluid velocity in the order of 60 m/s.

The present simulations required about 4 CPU seconds per physical time step. An average of about 25 sub-iterations have been necessary to converge the solution at each physical time step. The simulations, performed on an 8 processor, 2.33 GHz clock frequency computer, have been run until the instantaneous torque values showed a deviation of less than 1% compared with the corresponding values of the previous period. Total CPU time has been about 2 days for each simulation.

VI. RESULTS AND DISCUSSION

Fig. 12 represents the average power coefficients for the two models, defined as:

$$C_p = P / (\tfrac{1}{2} \rho A V_\infty^3) \qquad (1)$$

for an incident wind speed of 9 m/s, as a function of the tip speed ratio, defined as:

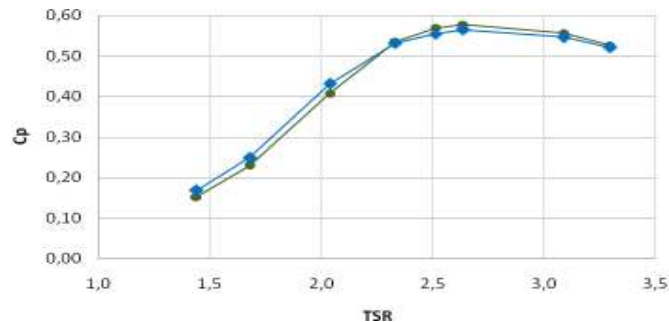$$TSR = \omega R_{rotor} / V_\infty \qquad (2)$$

Fig. 12 Comparison between rotor Model 1 (blue) and Model 2 (green) power curves for a wind speed at test section entrance of 9 m/s (correction due to blockage has not been considered).

The high value of the numerically determined maximum power coefficient (0.56) is fictitious and is due to wind tunnel blockage effects: the presence of an obstacle (the rotor) inside the wind tunnel test section raises the wind speed close to the rotor to a higher value than the unperturbed reference wind speed of 9 m/s, which was measured at the test section entrance. Anyway, being the blockage effect due to wind tunnel the same for the two analized rotors, the simulations allow the comparison between the two candidate blade geometric sections. The following remarks can be drawn:

- *Model 1* and *Model 2* show the same position of optimum tip speed ratio, being this parameter more connected with rotor solidity than with blade geometrical section;
- *Model 2* maximum C_p value (0.576) is 2% higher than *Model 1* corresponding value (0.565).
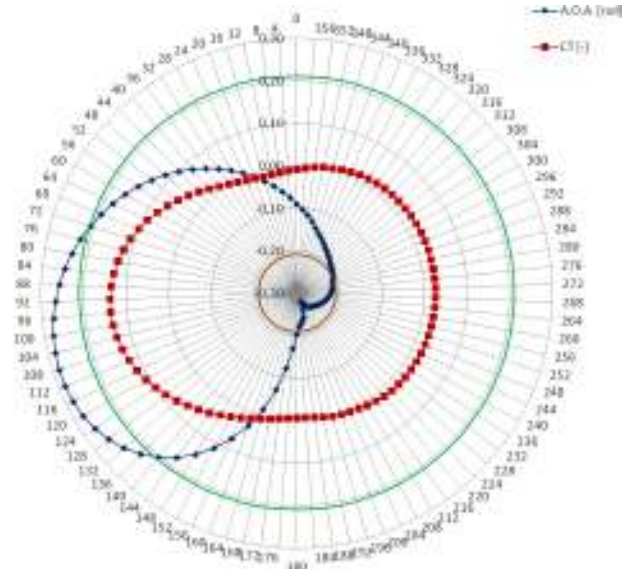

Fig. 13 Evolution of torque coefficient and of angle of attack as a function of blade azimuthal position for a single rotor blade (*Model 1*)
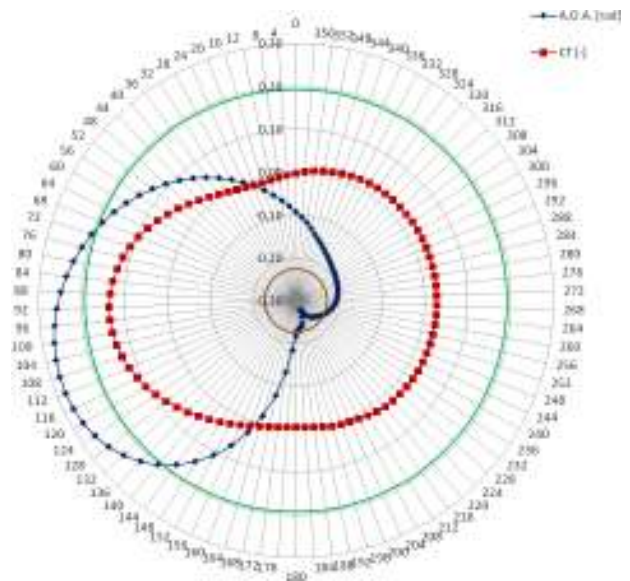

Fig. 14 Evolution of torque coefficient and of angle of attack as a function of blade azimuthal position for a single rotor blade (*Model 2*)

Figs. 13 and 14 show the distribution of the instantaneous torque coefficient, defined as:

$$C_T(\theta) = T(\theta) / (\tfrac{1}{2} \rho A R_{rotor} V_\infty^2) \qquad (3)$$

as a function of azimuthal position of rotor *Model 1* and *Model 2*, for a single rotor blade and for optimum tip speed ratio (TSR = 2.63). The angle between the relative velocity and the tangent to the blade trajectory at each azimuthal position was also determined as:

World Academy of Science, Engineering and Technology
International Journal of Aerospace and Mechanical Engineering
Vol:5, No:12, 2011

$$\alpha = \text{arctg} \ [U \sin\gamma \ / \ (U \cos\gamma - U_t)] \qquad (4)$$

being:

$$\gamma = \theta - \delta \qquad (5)$$

$$\delta = \text{arctg} \ (U_y/U_x) \qquad (6)$$

as proposed by Raciti Castelli et al. [12]. For further information on the adopted performance analysis, based upon a simplified aerodynamic model, consisting in the analysis of kinematic and dynamic quantities every 4° rotor azimuthal position along blades trajectory, see [12].
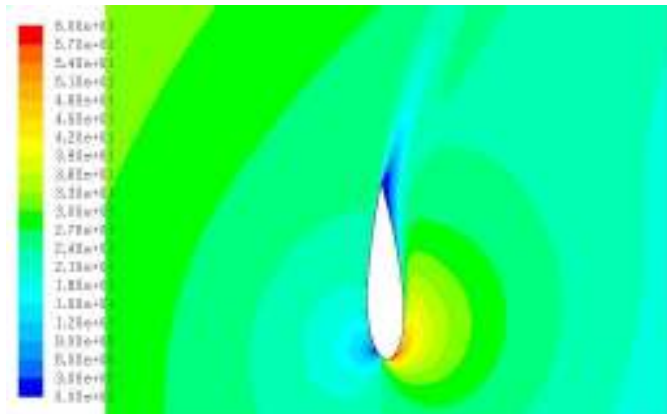

Fig. 15 Relative velocity contours for NACA 0021 blade section passing through 92° azimuthal position (wind is coming from the left) for optimum tip speed ratio (TSR = 2.63)
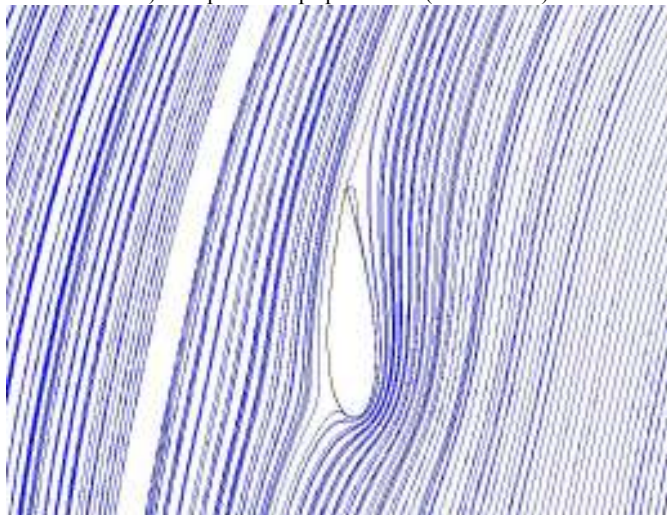

Fig. 16 Relative pathlines for NACA 0021 blade section passing through 92° azimuthal position (wind is coming from the left) for optimum tip speed ratio (TSR = 2.63)

As can be clearly seen, the maximum torque values are generated during the upwind revolution of the turbine and for azimuthal position where rotor blades are experiencing very high relative angles of attack, even beyond the stall limit, as can be seen in Figs. 15 and 26, representing a NACA 0021 blade section passing through 92° azimuthal position.
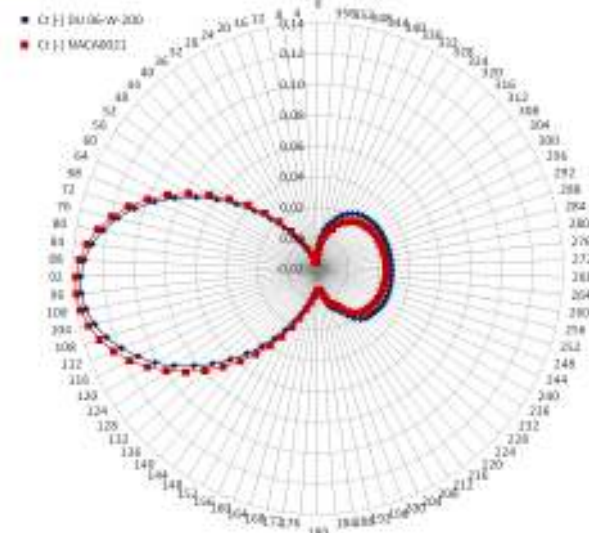

Fig. 17 Comparison between rotor Model 1 (red) and Model 2 (blue) instantaneous torque coefficient for a single rotor blade and for optimum tip speed ratio (TSR = 2.63); correction due to blockage was not considered
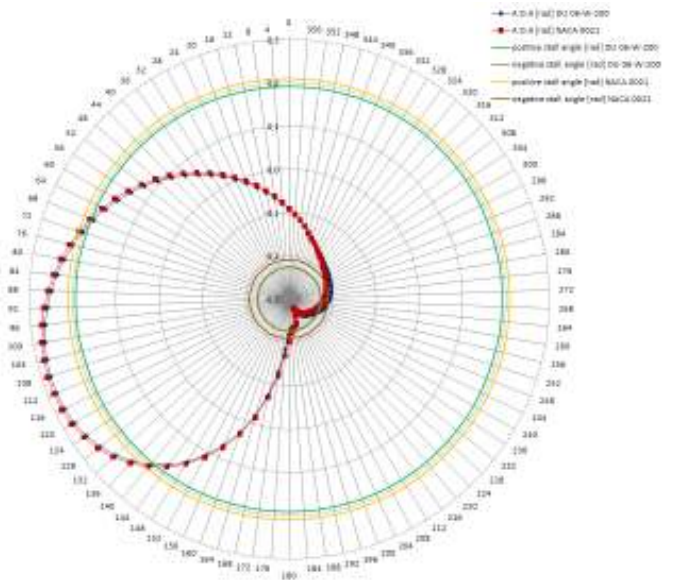

Fig. 18 Comparison between rotor Model 1 (red) and Model 2 (blue) istantaneous angle of attack for a single rotor blade and for optimum tip speed ratio (TSR = 2.63); correction due to blockage was not considered

As can be seen, for upwind azimuthal positions DU 06-W-200 performance is slightly lower if compared to NACA 0021, but for downwind azimuthal position the situation is quite the opposite and the overall balance is thus in favor of DU 06-W-200. This behavior is probably related to the slightly higher values of angles of attack experienced by DU 06-W-200 blade profile during downwind operation, as can be seen in Fig. 18.

World Academy of Science, Engineering and Technology
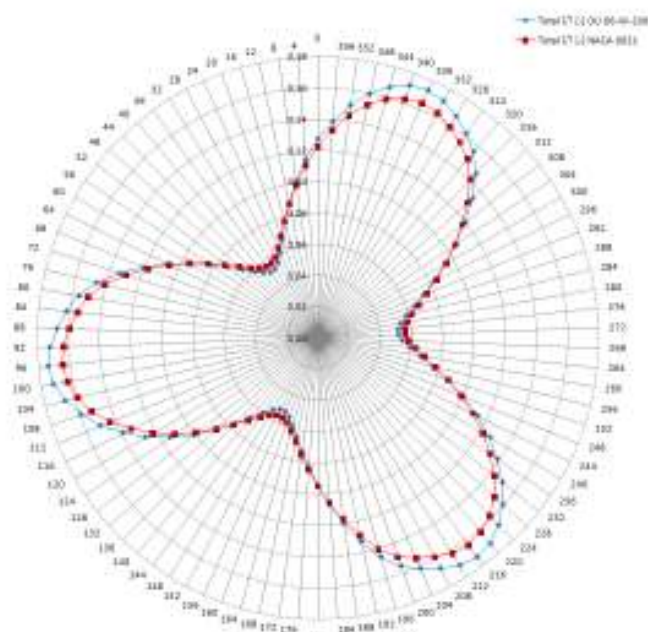International Journal of Aerospace and Mechanical Engineering
Vol:5, No:12, 2011

Fig. 19 Comparison between rotor Model 1 (red) and Model 2 (blue) instantaneous torque coefficient as a function of blade No. 1 azimuthal position

Fig. 19 shows a comparison between rotor *Model 1* and *Model 2* instantaneous torque coefficients as a function of blade No. 1 azimuthal position, for optimum tip speed ratio (TSR = 2.63). Once more, it can be clearly seen that torque values generated by DU 06-W-200 blade profile are higher than those obtained from NACA 0021, being these values the algebraic sum of each single blade contribution.

VII. CONCLUSION AND FUTURE WORK

In this paper a model for the evaluation of energy performance and aerodynamic forces acting on a small straight bladed Darrieus type vertical axis wind turbine depending on blade geometrical section has been developed, based on an analytical code coupled to a solid modeling software which was linked to a finite volume CFD code for the calculation of rotor performance.

The obtained results, based on two candidate blade profile architectures, which are characterized by a conventional NACA 0021 blade profile and a newly developed DU 06-W-200 non-symmetric profile, demonstrate the better performance of the latter. The increased DU 06-W-200 overall aerodynamic performance (up to nearly 2% with respect to NACA 0021) is due to an increased blade performance during downwind operation: even though the maximum torque values are generated during the upwind revolution of the turbine, downwind blade operation has proved to be determining in improving DU 06-W-200 rotor aerodynamic behavior.

Finally, it has been proved that the maximum torque values generated during the operation of a vertical axis wind turbine blade correspond to azimuthal position where rotor blades are experiencing very high relative angles of attack, even beyond the stall limit. Further work should be performed in order to investigate the behavior of the two proposed rotor architectures in open field conditions.

NOMENCLATURE

A [m^2]	rotor swept area
c [mm]	blade chord
C_p [-]	rotor average power coefficient
$C_T(\theta)$ [-]	rotor instantaneous torque coefficient
R_{rotor} [mm]	rotor radius
H_{rotor} [mm]	rotor height
N [-]	number rotor of blades
s [mm]	blade thickness
$T(\theta)$ [Nm]	rotor instantaneous torque
T.S.R. [-]	tip speed ratio
V_∞ [m/s]	unperturbed wind velocity at computational domain entrance
α [°]	blade angle of attack
TSR [-]	tip speed ratio
U [m/s]	absolute wind velocity at blade position
U_t [m/s]	blade tangential speed at blade position
U_x [m/s]	absolute wind velocity at blade position, component along x axis
U_y [m/s]	absolute wind velocity at blade position component along y axis
δ [°]	angle between absolute wind velocity at blade position and unperturbed wind direction
γ [°]	angle between absolute wind velocity at blade position and blade translational speed at blade position
θ [°]	blade azimuthal coordinate
ρ [kg/m3]	unperturbed air density (assumed 1.225)
σ [-]	rotor solidity
ω [rad/s]	rotor angular velocity

REFERENCES

[1] Glauert, H., "Airplane Propellers", *Aerodynamic Theory, Dover Publication Inc*, New York, 1963, Vol. 4, Division L, 169-360.
[2] Templin, R. J., "Aerodynamic Performance of Vertical-Axis Wind Machines", *ASME Paper 75-WA/ENER-1*, 1975;
[3] Strickland, J. H., "The Darrieus Turbine: A Performance Prediction Model Using Multiple Streamtube", *SAND75-0431*;
[4] Sheldal, R. E., Klimas, P. C., "Aerodynamic Characteristics of Seven Symmetrical Airfoil Sections Through 180-Degree Angle of Attack for Use in Aerodynamic Analysis of Vertical Axis Wind Turbines", *SAND80-2114*, Unlimited Release, UC-60;
[5] Burton, T., Sharpe, D., Jenkins, N., Bossanyi, E., *Wind Energy Handbook*, John Wiley & Sons, Ltd, 2001;
[6] Stathopoulos, T., "Wind Effects on People", *Proceedings of the International Conference on Urban Wind Engineering and Building Aerodynamics – Impact of Wind Storm on City Life and Built Environment*, COST Action C14, Von Karman Institute, Rode-Saint-Genèse (Belgium), 2004;
[7] Jensen, A. G., Franke, J., Hirsch, C., Schatzmann, M., Stathopoulos, T., Wisse, J., Wright, N. G., "CFD Techniques – Computational Wind Engineering", *Proceedings of the International Conference on Urban Wind Engineering and Building Aerodynamics – Impact of Wind and Storm on City Life and Built Environment* – Working Group 2, COST Action C14, Von Karman Institute, Rode-Saint-Genèse (Belgium), 2004;

[8] Raciti Castelli, M., *Analisi numerica delle prestazioni di una micro-turbina eolica ad asse verticale modello Darrieus*, PhD Thesis (in Italian), Università di Padova, Italy, 2010, pp. 193-194;

[9] Simao Ferreira, C. J., Bijl, H., van Bussel, G., van Kuik, G., "Simulating Dynamic Stall in a 2D VAWT: Modeling Strategy, Verification and Validation with Particle Image Velocimetry Data", *The Science of Making Torque from Wind*, Journal of Physics: Conference Series 75, 2007;

[10] Simao Ferreira, C.J., van Bussel, G., Scarano, F., van Kuik, G., "2D PIV Visualization of Dynamic Stall on a Vertical Axis Wind Turbine", *AIAA, 2007*;

[11] Raciti Castelli, M., Benini, E., "Effect of Blade Inclination Angle on a Darrieus Wind Turbine", *Journal of Turbomachinery*, May 2011, Vol. 134, 031016-1-10.

[12] Raciti Castelli, M., Englaro, A., Benini, E., "The Darrieus Wind Turbine: Proposal for a New Performance Prediction Model Based on CFD", *Energy 36* (2011) 4919-4934.

[13] Raciti Castelli, M., Villa, A., Benini, E., "CFD Analysis of the Influence of Central Shaft on Vertical-Axis Wind Turbine Noise Emission", *Fourth International Meeting on Wind Turbine Noise*, Rome, Italy, 12-14 April 2011.

[14] Claessens, M. C., *The Design and Testing of Airfoils for Application in Small Vertical Axis Wind Turbines*, Master of Science Thesis, Faculty of Aerospace Engineering, Delft University of Technology, November 9th, 2006.

[15] Abbott, H., Von Doenhoff, A. E., *Theory of Wing Sections*, Dover Publications, New York, 1959.

[16] http://www.windtunnel.polimi.it/brochure.pdf

[17] Raciti Castelli, M., Ardizzon, G., Battisti, L., Benini, E., Pavesi, G., "Modeling Strategy and Numerical Validation for a Darrieus Vertical Axis Micro-Wind Turbine", *ASME International Mechanical Engineering Congress & Exposition*, Vancouver, British Columbia, Nov 12-18, 2010, IMECE2010-39548.

[18] Fluent Inc., *Fluent User's Manual*, pp. 52, 54, 59, 71, 143.

[19] Cummings, R.M., Forsythe, J.R., Morton, S.A., Squires, K.D., "Computational Challenges in High Angle of Attack Flow Prediction", 2003, *Progr Aerosp Sci* 39(5):369-384.